SUPPLEMENTARY INFORMATION

Shear-Sensitive Clustering of Nanoparticles and their Protein Corona Composition Govern α-Synuclein Aggregation

Masoumeh Zanganeh [1,2], Thomas O. Mason [2], Hoda Eskandari [3], Vibeizonuo Rupreo [2], Fatemeh Bagheri [1*], Azad Farzadfard [2], Seyed Abbas Shojaosadati [1], Dina Morshedi [4], Duncan S. Sutherland [3], Alexander K. Buell [2*] and Hossein Mohammad-Beigi [2*]

[1] Department of Biotechnology, Faculty of Chemical Engineering, Tarbiat Modares University, Tehran, Iran

[2] Protein Biophysics, Department of Biotechnology and Biomedicine, Technical University of Denmark, 2800, Kgs. Lyngby, Denmark

[3] Interdisciplinary Nanoscience Centre (iNANO), Aarhus University, 8000 Aarhus C, Denmark

[4] Bioprocess Engineering Research group, Institute of Industrial and Environmental Biotechnology, National Institute of Genetic Engineering and Biotechnology, Tehran, Iran

Corresponding authors: Fatemeh Bagheri (f.bagheri@modares.ac.ir), Hossein Mohammad-Beigi (hosmbe@dtu.dk) and Alexander K. Buell (alebu@dtu.dk)

Supplementary Figures

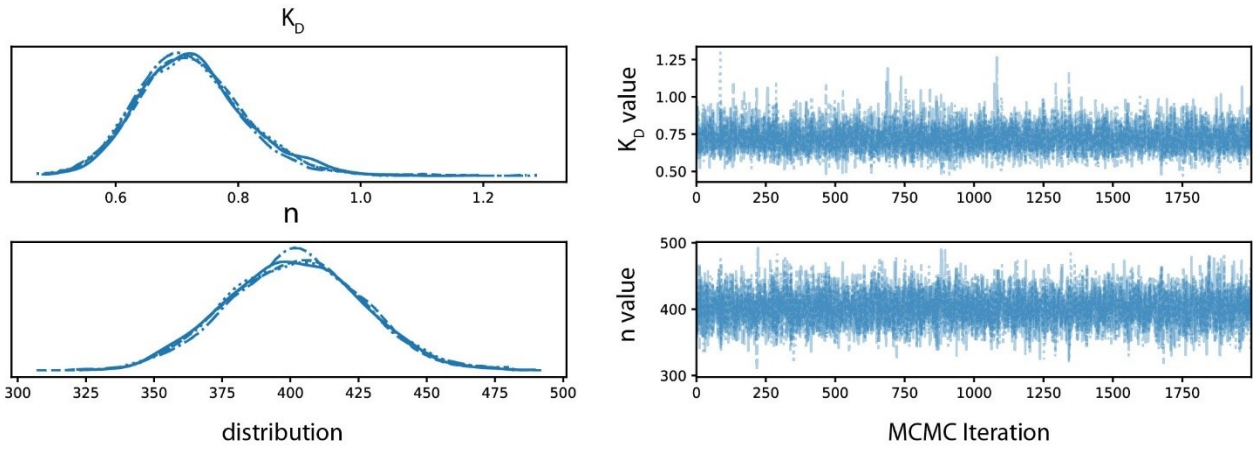

Figure S1. Trace plot of the posterior samples for Kd and n. The left panels display the posterior distributions of each parameter. The right panels show the sampling history (MCMC traces) indicating convergence and mixing.

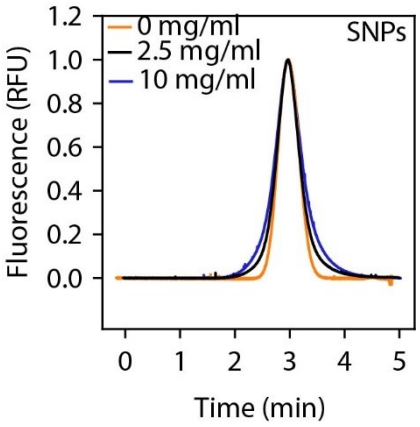

Figure S2. Evaluation of the interaction of αSyn and SNPs by FIDA. Taylograms of αSyn interacted with 0, 2.5, and 10 mg/ml SNPs.

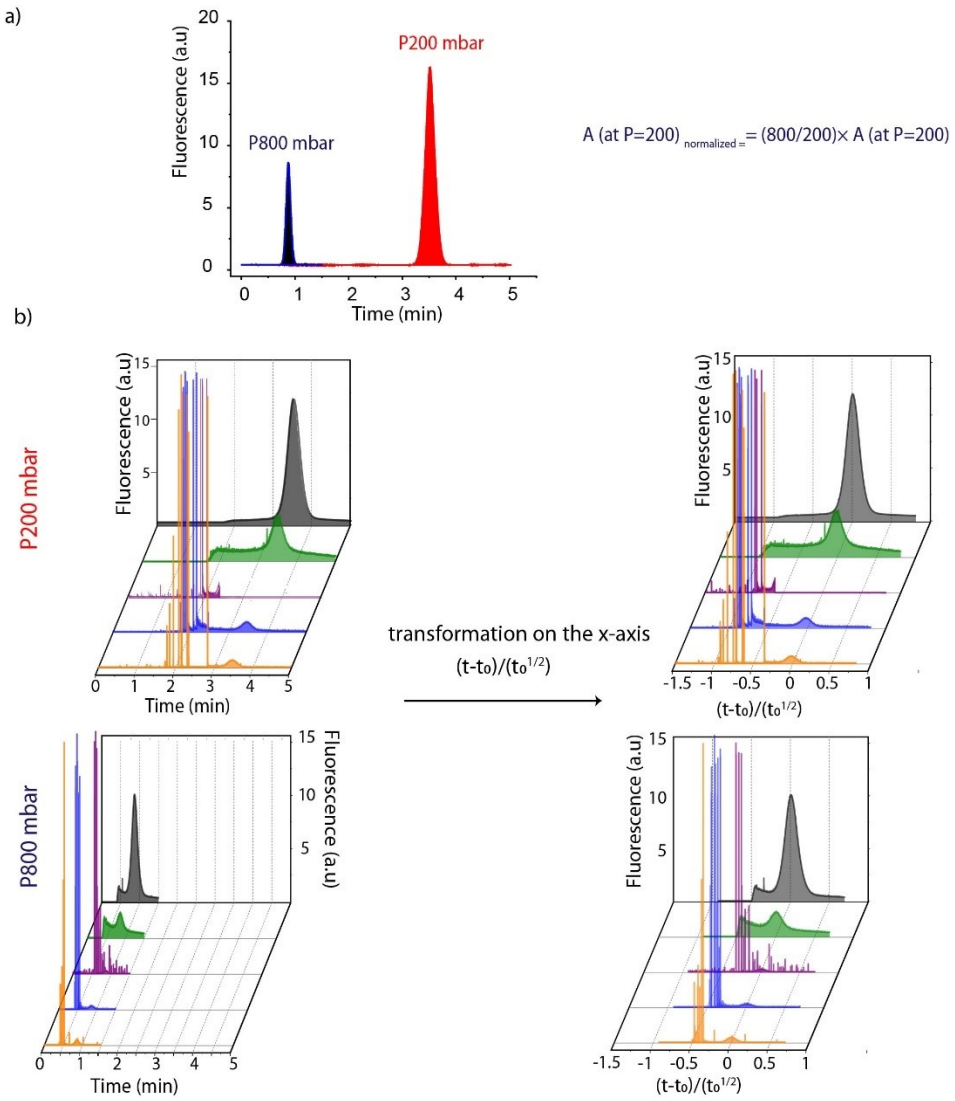

Figure S3. a) The protocol for normalizing the area compensates for the effect of pressure on signal intensity, which decreases at higher pressures due to increased particle velocity and reduced detection time. This effect scales linearly with pressure. b) Transformation of the x-axis was applied to correct for pressure-induced shifts, enabling direct comparison of signals. This transformation affects only the x-axis and does not alter the area under the signal.

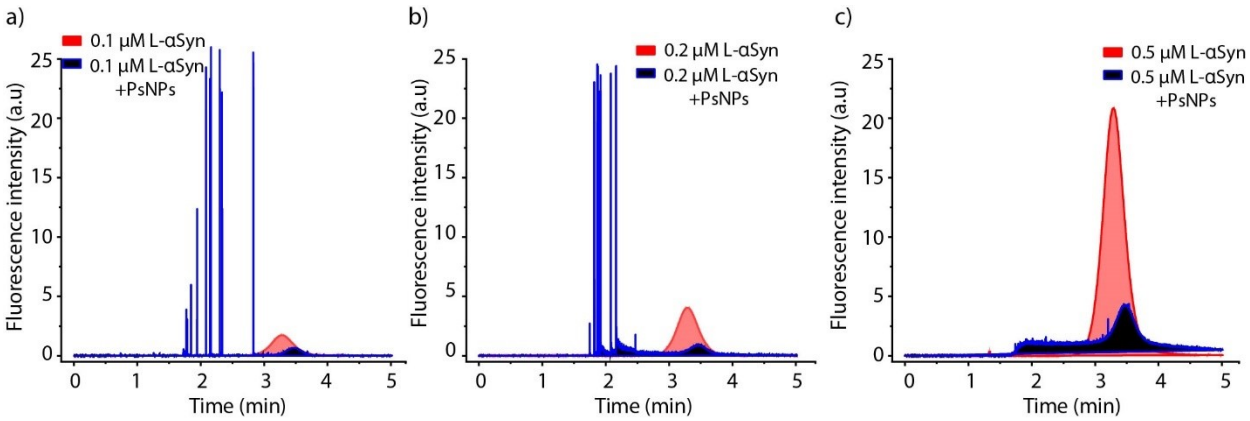

Figure S4. Interaction of L-αSyn (0.1, 0.2, and 0.5 µM) with PsNPs (0.1 mg/mL) in mode 1 at 200 mbar, as shown in Figure 4a. The TDA profile of L-αSyn in the absence of PsNPs is also shown for comparison, highlighting changes in the monomer signal before and after interaction with PsNPs, and illustrating the extent of protein binding to the NPs.

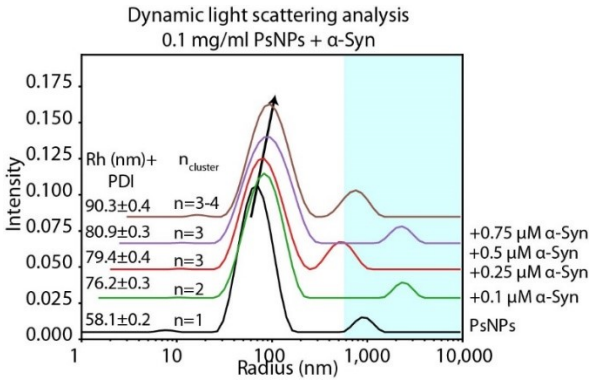

Figure S5. Dynamic light scattering (DLS) analysis of PsNPs (0.1 mg/mL) in the presence and absence of αSyn at varying αSyn concentrations (0, 0.1, 0.25, 0.5, and 0.75 µM). The cluster size, represented by n (the number of PsNPs in the clusters), was calculated using $R_n = \sqrt[3]{n} \times R_h$, where R_n is the measured hydrodynamic radius (nm) and R_h is the hydrodynamic radius without αSyn.

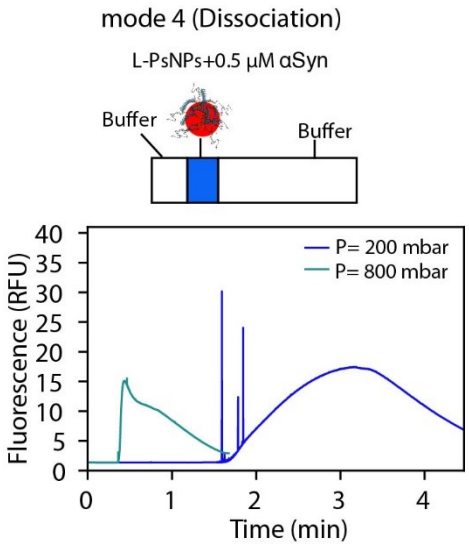

Figure S6. TDA of L-PsNPs interacting with αSyn (0.5 µM) at 200 and 800 mbar.

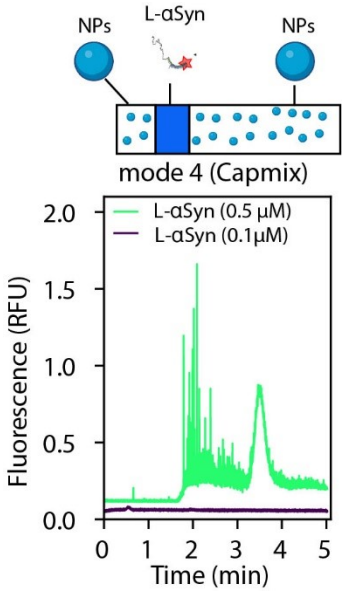

Figure S7. Interaction of L-αSyn with PsNPs in mode 4, Capmix. Mode 4 characterizes the dynamic interactions between L-αSyn and PsNPs under capillary mixing conditions.

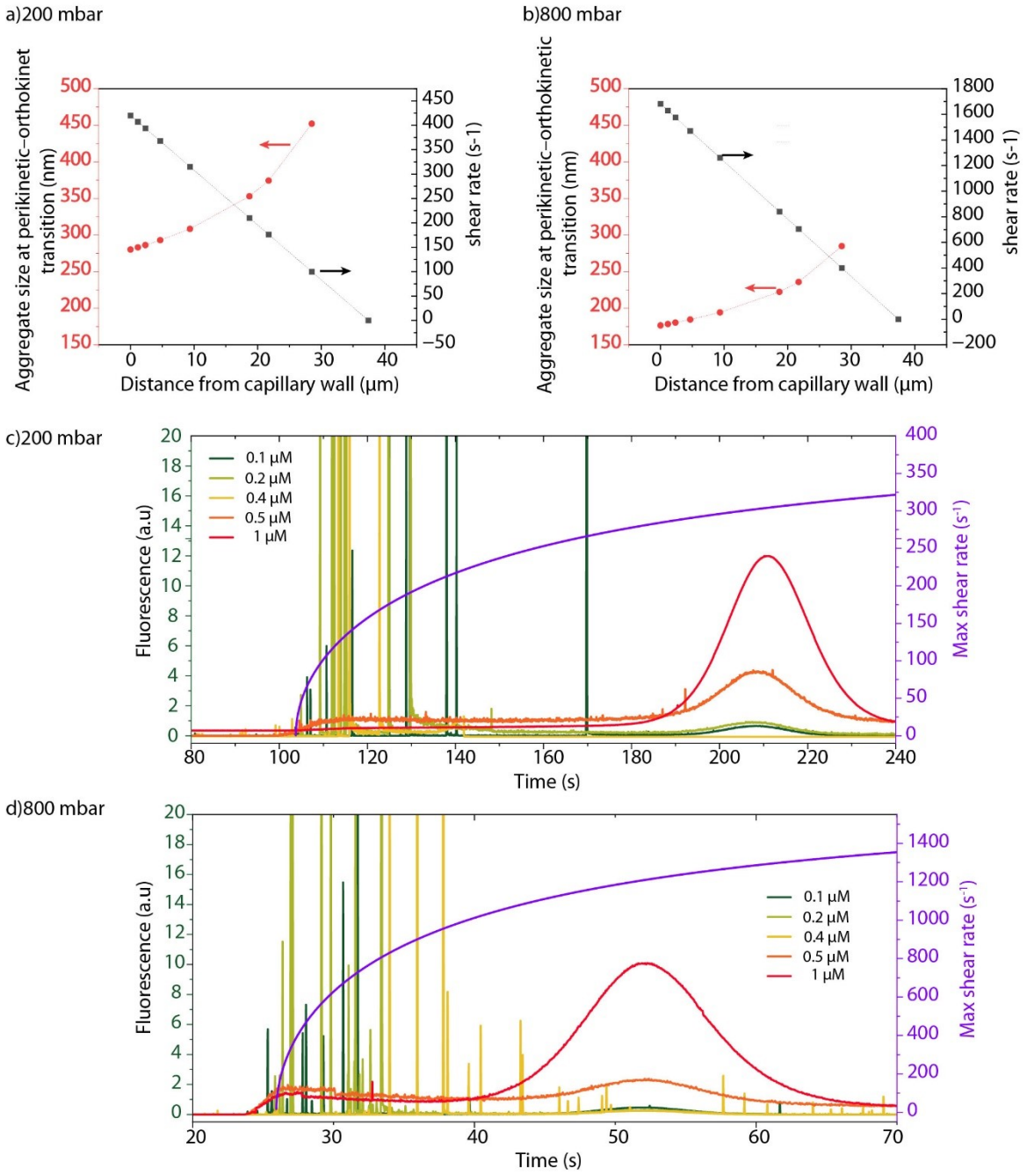

Figure S8. Aggregate size at perikinetic–orthokinetic transition at 200 mbar (a) and 800 mbar (b). Maximum shear rate (s^{-1}) calculated at different times and at two pressures: 200 mbar (c) and 800 mbar (d).

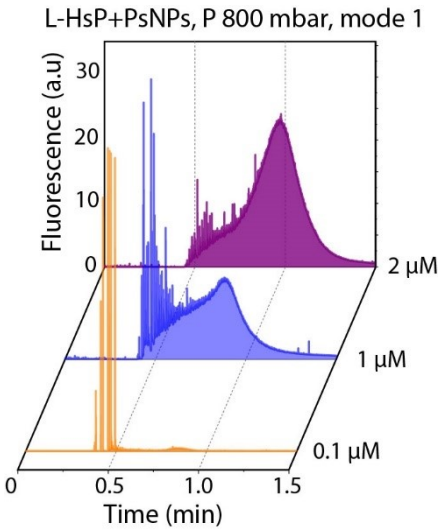

Figure S9. TDA of L- HsP interacting with PsNPs in mode 1 at 800 mbar.

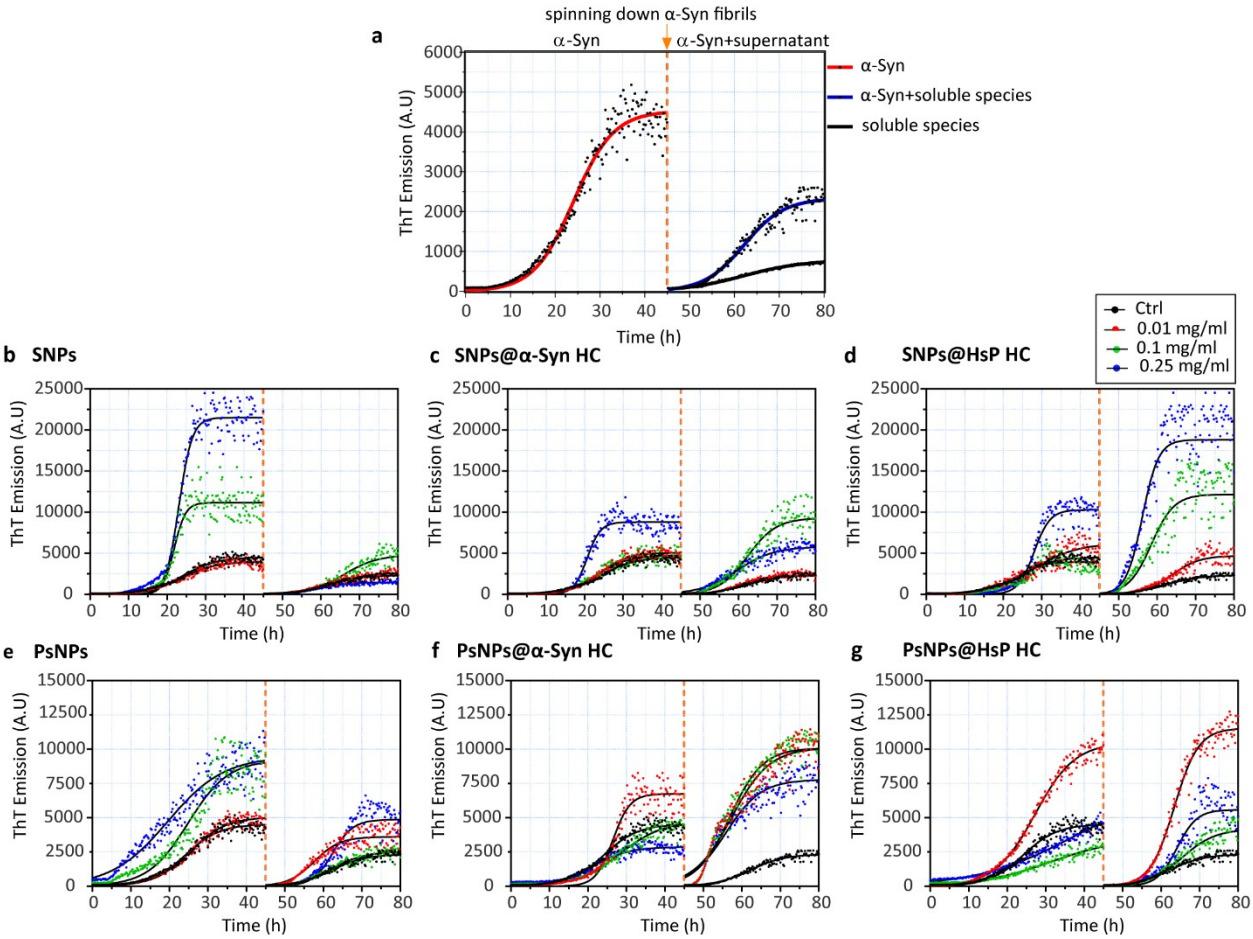

Figure S10. Kinetic time courses of αSyn aggregation before and after removal of NPs and fibrils formed prior to removal. (a) αSyn aggregation in the absence of NPs. (b- d) αSyn aggregation over time (hours) in the presence of pristine, αSyn HC, and HsP HC SNPs at different NP concentrations (0.01, 0.1, and 0.25 mg/mL). (e-g) αSyn aggregation over time in the presence of PsNPs at the same concentrations.

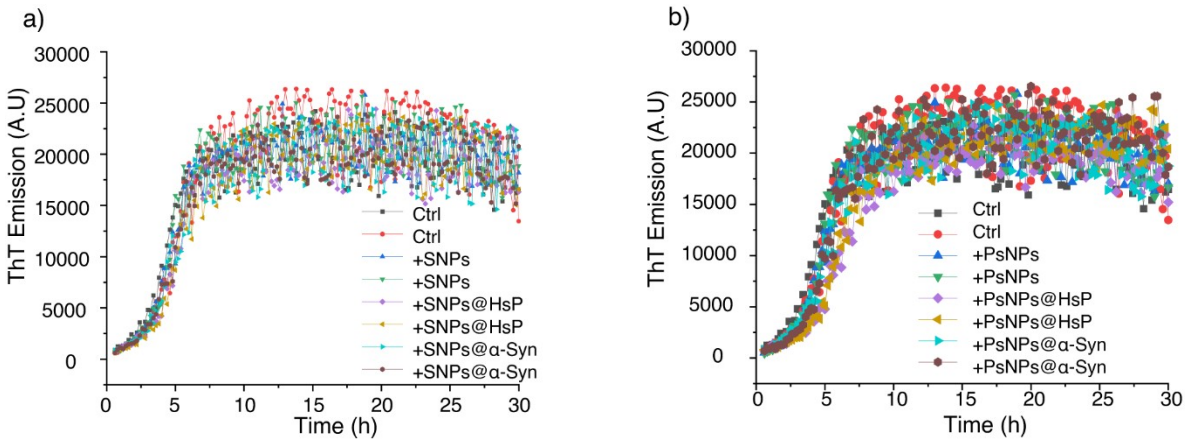

Figure S11. αSyn aggregation in the presence of 10 % αSyn seeds and 0.1 mg/ml (a) SNPs and (b) PsNPs with and without HC as a function of time.

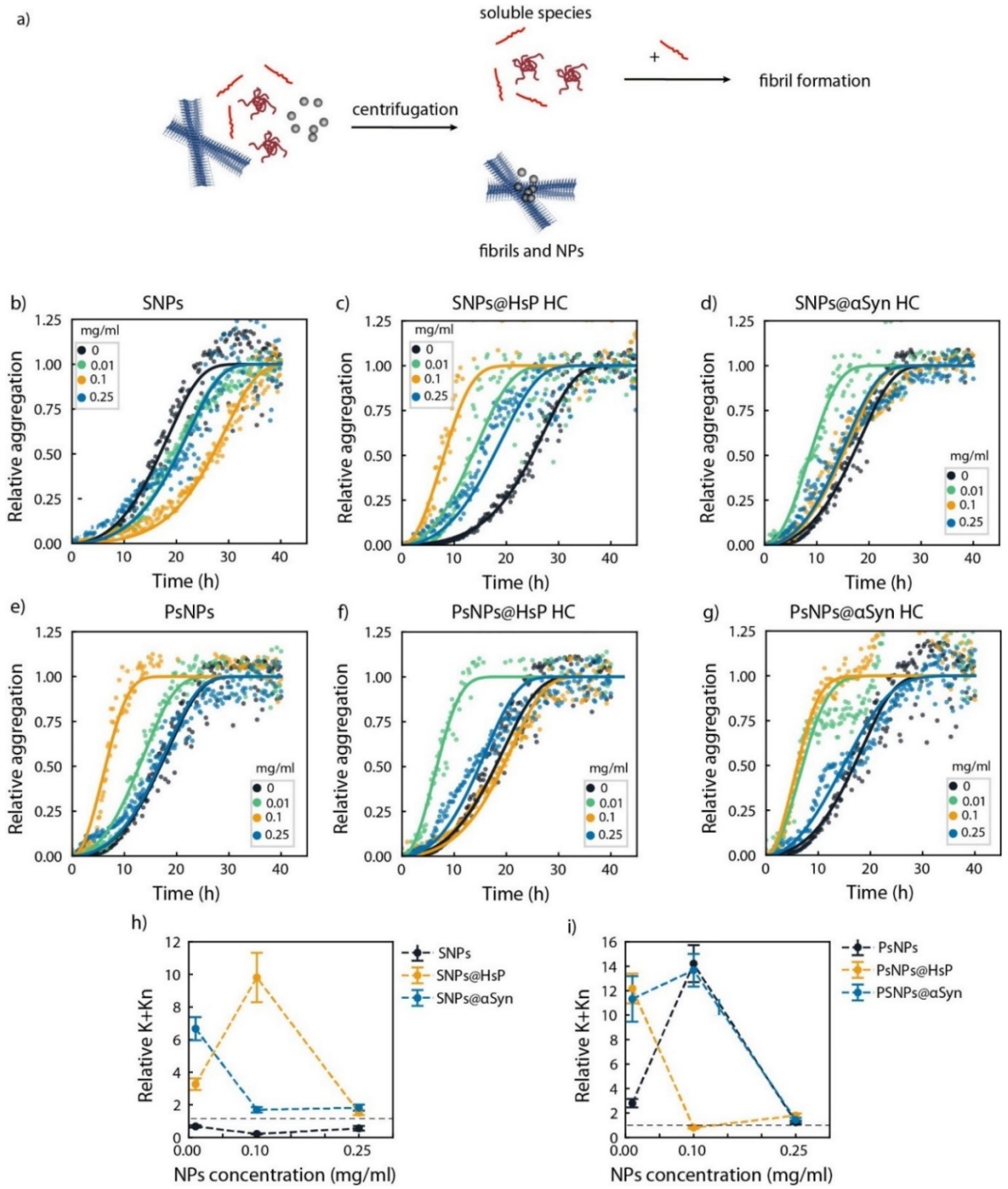

Figure S12. Normalized kinetic time courses of αSyn aggregation after the removal of NPs and fibrils formed during the first round, fitted with fibril formation models. (a) Schematic of the protocol used to remove fibrils and NPs. (b-g) Relative αSyn aggregation as a function of time in the presence of soluble species that were initially generated in the presence of pristine, HsP HC, and αSyn HC SNPs (b-d) and PsNPs (e-g) at different NP concentrations (0.01, 0.1, and 0.25 mg/mL) during the first round, followed by removal of the NPs and fibrils. Fresh monomer was added to the supernatant containing the soluble species, and fibrillation continued. The data were fitted to the fragmentation-dominated model, and joined lines represent the model's predictions. (h-i) Plots of relative $k_n k_+$ of fibril formation versus NPs concentration for αSyn fibril formation in the presence of the SNPs (h) and PsNPs (i). The original non-normalized data are shown in Figure S10.

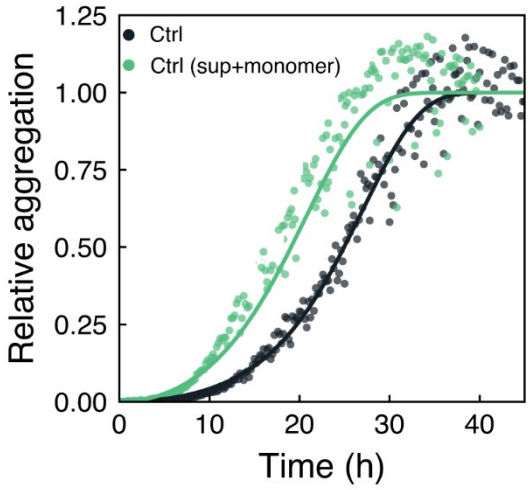

Figure S13. Normalized kinetic time courses of αSyn aggregation fitted with fibril formation models. Relative α-Syn aggregation after removal of fibrils as a function of time (h). Joined lines show the fragmentation-dominated model.

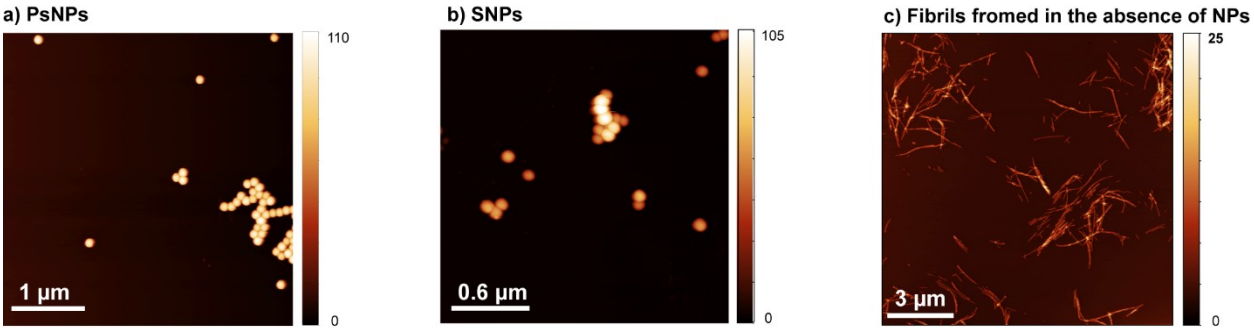

Figure S14. Atomic force microscopy (AFM) analysis. (a) PsNPs, (b) SNPs, and (c) fibrils formed in the absence of NPs.

Supplementary Notes

We calculated collision rates due to both perikinetic (diffusive) and orthokinetic (flow-induced) collisions. Our analysis showed that for primary particles (unbound nanoparticles), the rate of diffusion-induced collisions per unit volume was significantly higher than the rate of flow-induced collisions, with a difference of a factor of 10,000 divided by the local shear rate (at a 0.1 mg/ml NP concentration). This suggests that, at typical NP concentrations and on short timescales, perikinetic collisions dominate the aggregation process. However, the orthokinetic collision rate scales more strongly, i.e. with the cube of the sum of the radii of the particles, indicating that as NP aggregates and their size increases, flow-induced collisions may become more prominent and eventually dominant. Once a certain aggregation number is reached, perikinetic aggregates may transition to orthokinetic growth, where the shear forces of the flow play a more significant role in driving further aggregation.

The orthokinetic collision rate J_{ok} is given by:

$$J_{ok} = \left(\frac{4}{3}\right) n_1 n_2 (r_1 + r_2)^3 \gamma$$

where n_1 and n_2 are the number concentrations of the colliding particles (in particles/m^3), r_1 and r_2 are their radii, and γ is the shear rate (velocity gradient, in s^{-1}).

The perikinetic collision rate J_{pk} is given by:

$$J_{pk} = 4\pi D_{np} n_1 n_2 (r_1 + r_2)$$

where D_{np} is the relative diffusion coefficient of the two particles (m^2/s).

These two collision rates become equal for a typical shear rate ~100 s^{-1}, which corresponds to collisions between a single floc of radius r_2 and n_1 primary particles. The condition for equality is:

$$\frac{J_{ok}(f,1)}{J_{pk}(f,1)} = \frac{\mu\gamma(r_1 + r_2)^3}{2k_B T} = 1 \text{ where } (r_1 + r_2) = \sqrt[3]{\frac{2k_B T}{\mu}} \cdot \gamma^{-\frac{1}{3}}$$

where from the Stokes-Einstein equation we have $D_{np} = \frac{k_B T}{6\pi\mu r}$ and the mutual diffusion coefficient is the sum of the individual diffusivities $D_{np} = D_1 + D_2 = \frac{k_B T}{6\pi\mu}\left(\frac{1}{r_1} + \frac{1}{r_2}\right)$ and by assuming the aggregates of equal size $r_1 = r_2$. For primary particles of radius 50 nm and a shear rate of 100 s^{-1} (typical of central capillary flows in this experiment), the rates are equal when the floc radius is in the range of 350-400 nm.

The suppression of spikes outside of the "leading edge" of the distribution has two potential causes- firstly, the asymmetric form of the "transient", or non-Taylor dispersion, and the increased shear away from the capillary axis, which may lead to mechanical separation of large aggregates.

A significant excess viscosity was noted in aggregating systems for 0.1 mg/ml PsNPs (100 nm), the volume fraction of the primary particles is of the order $1x10^{-4}$. Calculation:

$$Vp = \frac{Mass}{density} = \frac{0.1\ mg}{1005\ mg/cm^3} = 9.52 \times 10^{-5} cm^3$$

$$\emptyset = \frac{Vp}{Vtotal} = \frac{9.52 \times 10^{-5} cm^3}{1\ cm^3} = 9.52 \times 10^{-5}$$

Here, $\emptyset = 9.52 \times 10\text{-}5$, gives a 0.024% increase in viscosity, which would be considered negligible. However, the viscosity shifted by a factor of 1.06, suggesting a much higher final volume fraction of around 2.4%, which is much larger than the calculated volume fraction of 0.024%. $\mu = \mu_0(1 + 2.5\emptyset)$. This excess viscosity could be due to the fractal nature of the aggregating flocs (aggregates of particles), which can form structures that take up more space and lead to a higher apparent volume fraction.
For fractals, the scaling of the floc hydrodynamic radius with aggregation number is governed by the following relationship: $\phi \propto A^{-1}\left(A^{\frac{1}{d}}\right)^3 = A^{\frac{3}{d}-1}$

For a fractal dimension d<3, the volume fraction of particles depends on their aggregation number. Conservation of mass ensures a constant flux of primary particles through the detector, independent of their aggregation state. At a pressure of 800 mbar, the flow rate is approximately $1.2x10^7$ particles per second, corresponding to roughly 4×10^5 particles during a 30 ms spike. The narrow distribution of spike widths and their strong clustering near the fast-flow region, corresponding to the low-shear zone at the center of the channel, suggests that shear plays a limiting role in particle size development.

The laminar flow in the capillary enables plotting of the shear experienced by particles as a function of their plug arrival time ((Figure S7c and S7d)). In fast-flow experiments, spike signals are suppressed above a critical shear threshold (~1000 s^{-1}), with the exception of a notable response at 0.4 μM (yellow trace). At 0.5 μM, the signal is characterized by numerous small, distinct spikes that diminish in intensity over time.

Assuming that flocs disintegrate at a shear rate of 1000 s^{-1}, and approximating shear forces acting on a homogeneous, uniform sphere, we estimate the effective floc volume fraction from the viscosity shift shown in Figure S3. For a floc containing 10^5 particles, a scaling exponent of 2.05 is obtained, implying a floc

radius of approximately 14 μm, large enough to span a significant portion of the capillary. The shear strength of such a floc can be estimated from:[1]:

$$\tau_b = 1.1\frac{\alpha^{d-3}}{1-\alpha^{d-3}} \cdot \frac{F}{4r_1^2}$$

where α is the ratio of floc to primary particle radius. The shear rate at breakup of the floc is then [2]:

$$\frac{\tau_b}{5\mu} \approx 1000 s^{-1}$$

giving a force between primary particles O~100pN, which is a reasonable estimate for a Hamaker constant of $10^{\wedge -20}$ J, particle diameter 10^{-7}m, and contact separation 1nm.

Repeating the analysis at a slower flow rate (ΔP = 200 mbar), we observe no spikes beyond a maximum shear rate of approximately 280 s^{-1}. While flocs formed under different shear conditions are known to exhibit variations in fractal dimensions, a more plausible explanation here is geometric: the floc's center of mass likely cannot approach the capillary wall more closely due to its large radius. A floc with an arrival time of 170 s under these conditions is traveling at a normalized radial position r r/R = 0.62, placing its center of mass roughly 9 μm from the wall, a value consistent with the predicted floc radius based on the previously discussed scaling exponent.

The persistence of flocs at 0.4 μM αSyn is particularly striking, suggesting a substantially higher interparticle attractive force. We propose that, consistent with the broader distribution of small peaks seen at 0.5 μM, the collision efficiency (i.e., the fraction of collisions that lead to successful incorporation into a floc) is significantly reduced at higher αSyn concentrations due to increased surface binding. This binding likely prevents close approach of particles in most cases. Nonetheless, occasional contact between uncoated surface regions remains possible, and in such instances, nanoparticles may be further stabilized by protein-mediated bridging interactions, where a single protein simultaneously binds to both surfaces at the contact site.

The disappearance of spikes in NP/protein FIDAgrams may thus serve as a sensitive indicator of surface saturation.

References

1 D. Wang, R. Wu, Y. Jiang and C. W. K. Chow, *Colloids Surf. Physicochem. Eng. Asp.*, 2011, **379**, 36–42.

2 D. F. Bagster and D. Tomi, *Chem. Eng. Sci.*, 1974, **29**, 1773–1783.